Tissue Eng Regen Med (2017) 14(5):631–639
DOI 10.1007/s13770-017-0057-y

Online ISSN 2212-5469
Print ISSN 1738-2696

ORIGINAL ARTICLE

Serial Analysis of Tracheal Restenosis After 3D-Printed Scaffold Implantation: Recruited Inflammatory Cells and Associated Tissue Changes

Hee-Jin Ahn[1] · Roza Khalmuratova[2] · Su A. Park[3] · Eun-Jae Chung[1] · Hyun-Woo Shin[1,2,4,5] · Seong Keun Kwon[1]

Received: 6 March 2017 / Revised: 4 April 2017 / Accepted: 17 April 2017 / Published online: 13 September 2017

Abstract Tracheal restenosis is a major obstacle to successful tracheal replacement, and remains the greatest challenge in tracheal regeneration. However, there have been no detailed investigations of restenosis. The present study was performed to analyze the serial changes in recruited inflammatory cells and associated histological changes after tracheal scaffold implantation. Asymmetrically porous scaffolds, which successfully prevented tracheal stenosis in a partial trachea defect model, designed with a tubular shape by electrospinning and reinforced by 3D-printing to reconstruct 2-cm circumferential tracheal defect. Serial rigid bronchoscopy, micro-computed tomography, and histology [H&E, Masson's Trichrome, IHC against α-smooth muscle actin (α-SMA)] were performed 1, 4, and 8 weeks after transplantation. Progressive stenosis developed especially at the site of anastomosis. Neutrophils were the main inflammatory cells recruited in the early stage, while macrophage infiltration increased with time. Recruitment of fibroblasts peaked at 4 weeks and deposition of α-SMA increased from 4 weeks and was maintained through 8 weeks. During the first 8 weeks post-transplantation, neutrophils and macrophages played significant roles in restenosis of the trachea. Antagonists to these would be ideal targets to reduce restenosis and thus play a pivotal role in successful tracheal regeneration.

Keywords Trachea · Restenosis · Inflammation · 3D-printing · Scaffold

1 Introduction

The trachea is a tube-like organ that connects the pharynx and larynx to the lungs, allowing the passage of air during respiration. Tracheal stenosis is a narrowing or constriction of the trachea that causes breathing problems. The most common symptom of tracheal stenosis is gradually worsening dyspnea, particularly when undertaking physical activities (exertional dyspnea). The patient may also experience added respiratory sounds, which in more severe cases can be identified as stridor. The causes of stenosis vary, and include congenital disease, injury, trauma, neoplasm, and infection. However, one of the most common

Hee-Jin Ahn and Roza Khalmuratova have contributed equally to this work.

✉ Hyun-Woo Shin
charlie@snu.ac.kr

✉ Seong Keun Kwon
otolarynx@snuh.org

[1] Department of Otorhinolaryngology-Head and Neck Surgery, Seoul National University Hospital, 101 Daehak-ro, Jongno-gu, Seoul 03080, Korea

[2] Obstructive Upper Airway Research (OUaR) Laboratory, Department of Pharmacology, Seoul National University College of Medicine, 103 Daehak-ro, Seoul 03080, Korea

[3] Department of Nature-Inspired Nanoconvergence Systems, Korea Institute of Machinery and Materials, Gajeongbuk-ro 156, Daejeon 34103, Korea

[4] Department of Biomedical Sciences, Seoul National University Graduate School, 103 Daehak-ro, Jongno-gu, Seoul 03080, Korea

[5] Cancer Research Institute and Ischemic/Hypoxic Disease Institute, Seoul National University College of Medicine, 103 Daehak-ro, Jongno-gu, Seoul 03080, Korea

causes of tracheal stenosis is long-term intubation [1, 2]. In recent years, the number of patients receiving intubation has increased because of increases in chronic and advanced diseases due to growth of the aging population and increases in preterm neonates with congenital birth defects that may not have survived before advances in medical technology. Long-term intubation causes ischemic necrosis of cartilage due to excessive pressure and induction of excessive proliferation of granulation tissue.

Various approaches have been tried for tracheal stenosis, such as surgical resection and reconstruction, balloon angioplasty, stent, irradiation, and laser treatment [3–6]. However, these methods have a number of disadvantages, making them less suitable for ultimate treatment of tracheal stenosis. Therefore, developing a new therapy to treat tracheal stenosis is regarded as a major goal of modern medicine.

Recently, tissue engineering approaches for reconstruction of the trachea have been actively pursued. Several studies have been conducted on tracheal reconstruction using scaffolds and a variety of stem cells. However, those studies have limitations for tracheal reconstruction due to overgrowth of granulation tissue (airway restenosis) and framework softening (airway collapse) [7]. To prevent excessive ingrowth of granulation tissue, we developed an artificial tracheal scaffold in the form of asymmetrically porous membrane (APM). The APM has pores of different sizes on the top and bottom to assist in free movement of cells at the bottom to enhance integration with host tissue, while limiting granulation ingrowth into the tracheal lumen at the top side. In our previous study, we used a partial tracheal defect model, which involved removal of one-third of the tracheal ring, and tracheal granulation was completely controlled with the APM [8, 9]. In a recent study, we attempted to extend this concept of tracheal reconstruction using APM in a circumferential defect model (i.e., 360° defect). In contrast to our expectations, all rabbits with the circumferential defect reconstructed with APM died of tracheal restenosis [10]. Other researchers also reported tracheal restenosis after transplanting the scaffold in large animal models that required long-term stenting [11, 12]. Tracheal restenosis has also been the main obstacle in human trials, because it requires repetitive procedures, such as multiple endoluminal stent placements, and thus remains the greatest challenge in tracheal regeneration [13].

Despite the importance of tracheal restenosis, there is a paucity of published data and few detailed investigations of its causes, histopathological changes after tracheal scaffold transplantation, or methods for prevention.

In other disease models, for example of chronic kidney disease, it has been shown that the degree and severity of damage and fibrosis are correlated with macrophage infiltration [14]. There is also growing evidence for a relationship between macrophages and myofibroblast activation during inflammation [15]. Myofibroblasts are generally recognized as the effector cells of fibrogenesis [16]. Myofibroblasts synthesize large amounts of extracellular matrix (ECM), which is mainly comprised of type I and III collagen fibers, fibronectin, laminin, and other basal membrane proteins that are the sources of scar tissue [17, 18]. In addition, myofibroblasts generate contractility, and distort the architecture of organs, due to the expression of smooth muscle proteins such as α-smooth muscle actin (α-SMA) [19].

In this study, a tracheal scaffold was developed by 3D-printing and transplanted into circumferential defects of the rabbit trachea. After transplantation, we investigated the inflammatory cells recruited in the restenosis process according to time point, and their effects on activated myofibroblasts, which are key mediators of fibrosis. This would play a vital role in successful tracheal transplantation in subsequent experiments and human trials by identifying ideal targets to reduce restenosis.

2 Materials and methods

2.1 Materials

Polycaprolactone (PCL; average MW = 45 kDa for rapid prototyping, 80 kDa for electrospinning) was purchased from Sigma-Aldrich (St. Louis, MO, USA). Chloroform (CF) was purchased from Junsei Chemical Co., Ltd. (Tokyo, Japan). Methanol (MeOH) was purchased from Daejung Chemicals & Metals Co., Ltd. (Shiheung, Korea). Deionized distilled water (DDW) was produced with an ultrapure water system (Puris-Ro800; Bio Lab Tech., Namyangju, Korea). All other reagents and solvents were of analytical grade and used without further purification.

2.2 Fabrication of tubular nanofibers via electrospinning

The fabrication of electrospun nanofibers (ENs) was performed as described previously [20, 21]. Briefly, PCL was dissolved in a mixed CF/MeOH (9:1) solvent to produce a 15 wt% solution. For electrospinning, the polymer solution was loaded into a Luer-Lok syringe attached to a blunt metal needle (20 G, Kovax-needle; Korea Vaccine Co., Ltd., Ansan, Korea) and a rotating mandrel with a diameter of 7 mm at 18 kV using a high-voltage DC power supply (Nano NC, Seoul, Korea) with a feed rate of 1 mL/h (KDS-200; KD Scientific Inc., Holliston, MA, USA) and a needle tip-to-collector distance of 15 cm. The resultant nanofiber was dried overnight under vacuum to remove any residual solvent.

2.3 Manufacture of tubular scaffold for tracheal regeneration by rapid prototyping

The 3D-printed PCL strands were fabricated as described previously [22]. Briefly, PCL pellets were melted at 100 °C in a heated dispenser. 3D-printed strands were extruded in a custom 3D printing system designed in our laboratory. The nozzle size and distance between strands were 300 and 300 μm, respectively. After melting of the PCL, a continuous air pressure of 300 kPa was applied to the dispenser, and strands of molten PCL were applied layer by layer onto the EN films. The 7-mm drum holding the EN film was rotated between layers to produce a patterned 0°/45° porous structure.

2.4 Animals and surgical procedures

Twelve male New Zealand white rabbits (Koatech Laboratory Animal Company, Pyeongtaek, Korea) weighing 2.6–3 kg were assigned to one of four groups as follows: (1) normal control (Group I); (2) 1 week after transplantation (Group II); (3) 4 weeks after transplantation (Group III); and (4) 8 weeks after transplantation (Group IV). All protocols were performed in accordance with the guidelines of the Animal Care Ethics Committee of Seoul National University Hospital (IACUC No. 15-0268-C1A1). Nine rabbits were anesthetized by intramuscular injection of Zoletil (50 mg/kg) and xylazine (4.5 mg/kg) and placed in the supine position. A vertical skin incision was made at the midline of the neck and the strap muscles were separated until the tracheal cartilage was exposed. A 2-cm circumferential tracheal defect was created for prosthesis placement. The scaffolds (20 mm in length) were sutured to cover the edges of the defects by approximately 1 mm on each side using 4-0 Vicryl (Johnson & Johnson, New Brunswick, NJ, USA). Finally, the strap muscles were sutured with 4-0 Vicryl and the skin was closed using 4-0 nylon sutures (Johnson & Johnson). Animals were observed for 2 h postoperatively before being returned to their cage, where water and standard feed were available. Over the following 7 days, each animal received kanamycin (20 mg/kg) as prophylaxis. Clinical signs were monitored daily, with special attention paid to weight, cough, sputum production, wheezing, and dyspnea. If there were signs of respiratory distress and weight loss more than 20% of the original body weight, the animal was euthanized.

2.5 Radiological evaluation using μCT and 3D reconstructed image

A micro-computed tomography (μCT) scanner (NFR Polaris-G90; NanoFocusRay, Jeonju, Korea) was used to identify the stenotic area of the trachea 8 weeks after scaffold transplantation. Six hundred μCT images were taken at settings of 65 kV, 60 mA, and 500 ms with a resolution of 512 × 512 in Digital Imaging and Communication in Medicine (DICOM) format. Three-dimensional images of each rabbit's larynx and trachea were reconstructed using Lucion software (Infinitt Healthcare, Seoul, Korea).

2.6 Histological analysis

Histological assessments were performed to evaluate the regenerative status of the operative side at 1, 4, and 8 weeks postoperatively. At completion of the study, the rabbits were sacrificed under deep anesthesia and their tracheas were harvested. Tracheal segments were fixed in 10% neutral formalin solution for 24 h at +4 °C. Fixed tissues were processed by dehydration through a graded series of ethanol, cleared in xylene, and then embedded in paraffin blocks using automated processing and embedding equipment. Sections were cut from blocks at a thickness of 4 μm and mounted onto slides.

The histological changes were determined by hematoxylin and eosin (H&E) staining for overall inflammation, and Masson's trichrome stain for fibroblast presence and collagen deposition. To determine the degree of inflammatory response, the sections were examined with a light microscope (400× magnification), and the numbers of infiltrating neutrophils, macrophages, and fibroblasts from five sampling areas were counted independently by two examiners blinded to the experimental groups. The fibroblast-like cell count was based on the presence of spindle-shaped cells and collagen deposition. The results regarding inflammatory cells and fibroblast infiltration were expressed as the number of cells per high-powered field. Stained sections were analyzed and photographed using an Olympus BX41 microscope (Olympus, Tokyo, Japan).

2.7 Immunohistochemistry

After deparaffinization, endogenous peroxidase activity was quenched with 3% hydrogen peroxide in MeOH for 10 min followed by microwave treatment in antigen retrieval solution (Dako, Glostrup, Denmark). Specimens were blocked with 3% bovine serum albumin (BSA) for 1 h at room temperature (RT) followed by incubation with primary antibody (1:100) diluted in blocking buffer overnight at +4 °C. Mouse monoclonal anti-α-SMA and mouse monoclonal anti-macrophage antibodies were obtained from Abcam (Cambridge, UK).

The specimens were incubated with the appropriate secondary antibody for 1 h (1:100 dilution), followed by an avidin–biotinylated enzyme complex for 1 h and then 3,3′-diaminobenzidine for 5 min at RT. Avidin–biotin complex

kits were obtained from Vector Laboratories (Burlingame, CA, USA). Slides were counterstained with Gill's hematoxylin for 3 min, dehydrated in a graded ethanol series, cleared in xylene and mounted in Permount (Fisher Scientific, Pittsburgh, PA, USA). Negative controls were prepared by omission of the primary antibody, and the absence of nonspecific staining was verified. α-SMA deposition was quantified using Image J software (National Institutes of Health, Bethesda, MD, USA). The selected area was divided by the whole tissue area in the same image to determine the percentile value of alpha-smooth muscle deposition.

2.8 Statistical analysis

Data are expressed as means ± standard deviation (SD). The nonparametric Mann–Whitney *U* test was used to analyze differences between groups. Statistical analyses and data plotting were performed using SigmaPlot (ver. 10; Systat Software, Richmond, CA, USA). In all analyses, $p < 0.05$ was taken to indicate statistical significance.

3 Results

3.1 μCT findings of the trachea

μCT images showed complete airway obstruction at the level of scaffold transplantation (Fig. 1A) compared with the patent airway of the normal trachea (Fig. 1B).

3.2 Histological changes over time

Normal mucous membrane consists of areolar and lymphoid tissue, and presents a well-marked basement membrane supporting a stratified epithelium, the surface layer of which is columnar and ciliated, while the deeper layers are composed of oval or rounded cells. H&E and Masson's trichrome staining revealed no evidence of epithelial damage or inflammatory cell infiltration in control rabbit tracheal specimens (Fig. 2A, B).

Histopathological analyses revealed various degrees of inflammatory changes in the rabbit tracheal tissue specimens around the implant over time. Postoperative histological assessment revealed tissue hypertrophy caused by accumulation of inflammatory cells, proliferation of fibroblasts, and thickened collagen fibers around the implant (Fig. 2A, B).

3.3 Infiltration of inflammatory cells over time

Specimens showed severe infiltration of inflammatory cells and granulation tissue formation into the tracheal lumen 1 week after the operation. As tissue was collected 1, 4, and 8 weeks post implantation, the later stages of the inflammatory response were captured, in which large populations of neutrophils and macrophages were present in all specimens (Figs. 3, 4). As shown in Fig. 4A, the distribution of macrophages in rabbit tracheal tissue specimens was determined by immunohistochemistry. Furthermore, the percentage of macrophage-positive cells tended to increase from week 4 to week 8. Taken together, these findings indicated that neutrophils and macrophages are the predominant leukocyte subsets that actively accumulate around the implant (Fig. 4B, C).

3.4 Fibrosis and fibroblast recruitment

We counted the numbers of fibroblasts, which are key players in the synthesis of fibrous connective tissue during the healing process. Masson's trichrome staining of tissue specimens revealed presence of fibroblasts at week 4 and accumulation of collagen deposition around the implant at week 8. Fibroblasts were observed in all test animals,

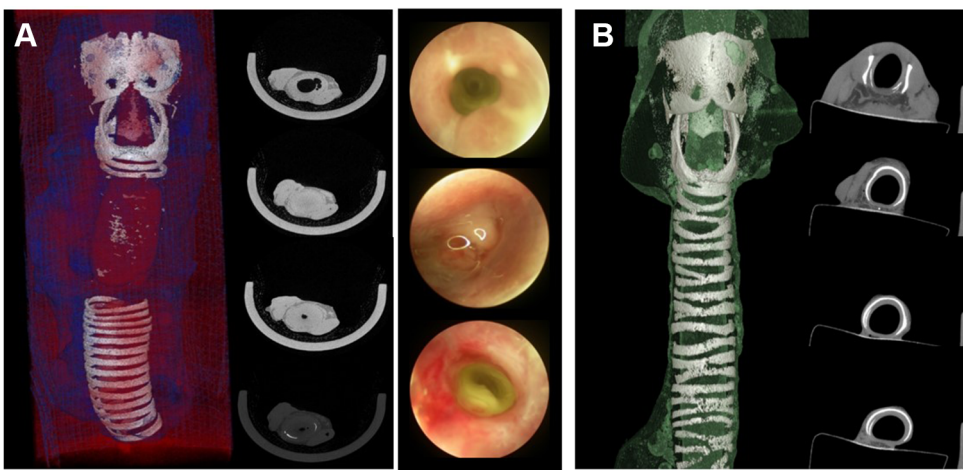

Fig. 1 **A** A 3D reconstructed image (*left*) and axial images of micro-computed tomography (μCT) at the level of scaffold transplantation. **B** A 3D reconstructed image (*left*) and axial μCT images of normal trachea

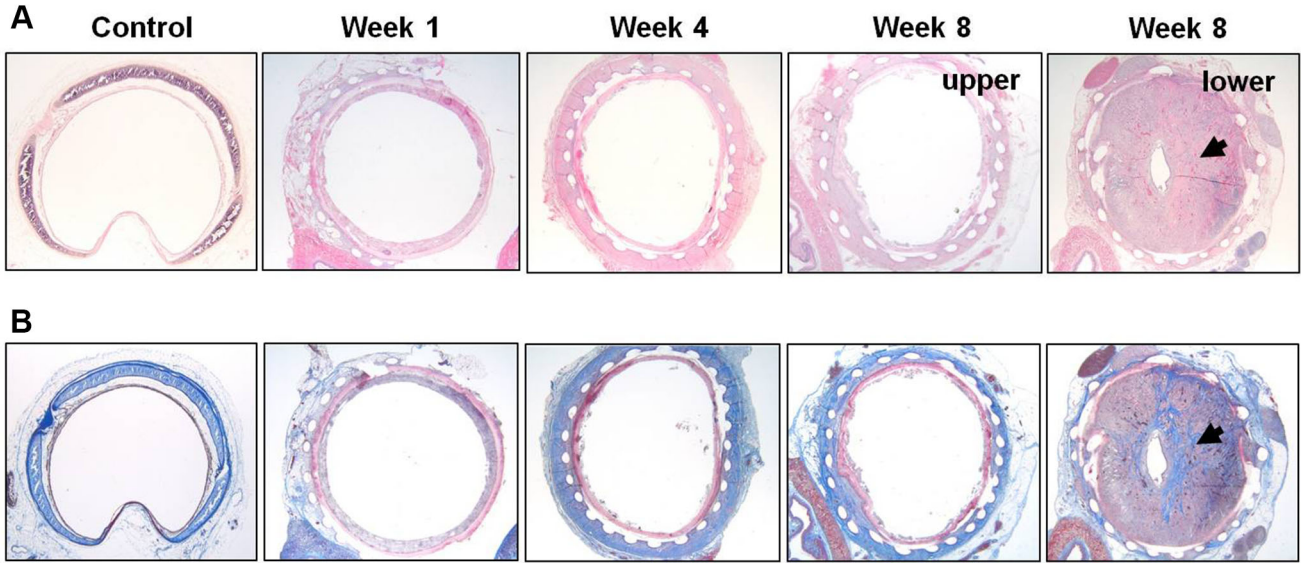

Fig. 2 **A** Hematoxylin-eosin (H&E) and **B** Masson's trichrome staining results of cross-sections of specimens taken 1, 4, and 8 weeks after implantation. A normal pseudostratified columnar ciliated epithelium was observed in the control group. The presence of inflammatory cells, predominantly neutrophils, within and around the implant at week 1. Histological examination showed inflammation around the implant with submucosal hyperplasia caused by proliferation of fibroblasts at week 4. At week 8, the outer layer of the implant was consistently covered with inflammatory cells and fibrosis (*arrows*)

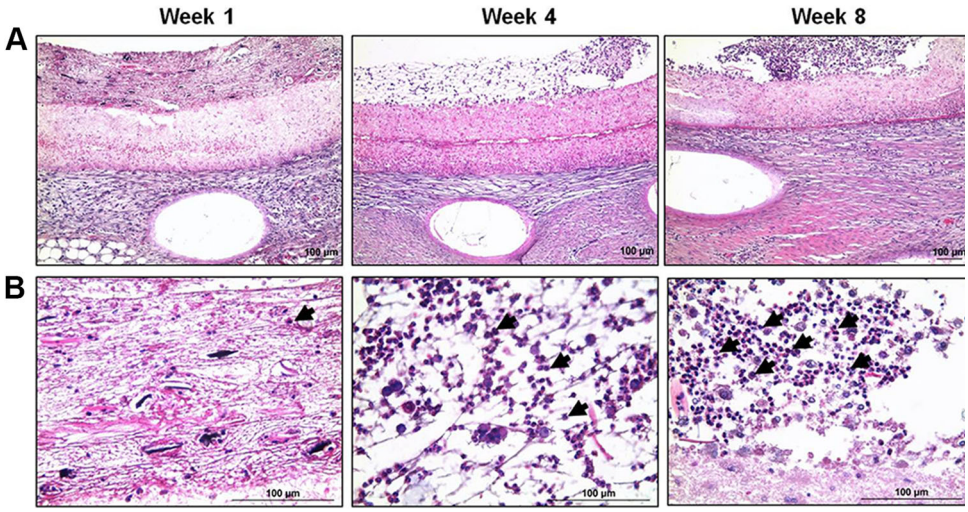

Fig. 3 **A** Representative images of tissue specimens showing histological evidence of a dense inflammatory infiltrate taken 1, 4 and 8 weeks after implantation (H&E staining). **B** Assessment of the cellular response to the tracheal scaffold revealed that acute inflammatory cells (neutrophils: arrow in week 1) and chronic inflammatory cells (mononucleated cells: *arrows* in week 4 and 8) were present around the implant according to time interval. Panel B represents a higher magnification of A. *Scale bars* in A and B = 100 μm

usually oriented in a layer around the scaffold (Fig. 5A, B). Eight weeks after surgery, dense fibrosis in the peritracheal area and protrusion of fibrotic tissue into the tracheal lumen, with no evidence of organized respiratory epithelium, were observed in each specimen. Histological analysis of the outer covering of the implant revealed diffuse fibrosis in all rabbits at week 8 (Fig. 2).

3.5 Immunohistochemical staining for α-SMA

As shown in Fig. 6 also examined the distribution of α-SMA by immunohistochemistry. The degree of α-SMA deposition increased at week 4 and week 8 as a result of fibroblast activation (Fig. 6A, B).

4 Discussion

Several clinical trials have been performed to prevent restenosis following tracheal reconstitution with a variety of methods [13, 23–25]. However, these were not optimal solutions because repeated performance of procedures was required after transplantation to control restenosis, which subsequently resulted in high costs, and inconvenience

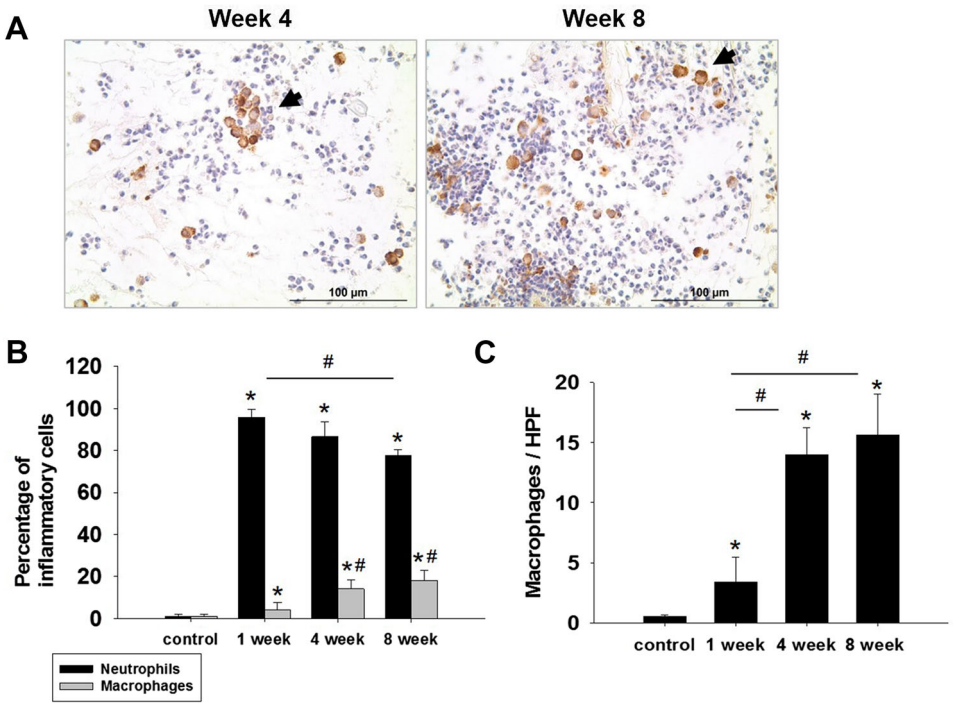

Fig. 4 **A** Immunohistochemical detection of macrophages and **B, C** evaluation of inflammatory cell quantity. Representative photomicrographs of tissue sections demonstrating increased macrophage infiltration at 4 and 8 weeks after implantation. Macrophage-positive cells are indicated by *arrows* and quantified per high-powered field (HPF; **A**–**C**). Data are expressed as means ± SD. $*p < 0.05$, compared to the control group; $\#p < 0.05$ compared to week 1; Mann–Whitney *U* test. *Scale bar* = 100 μm

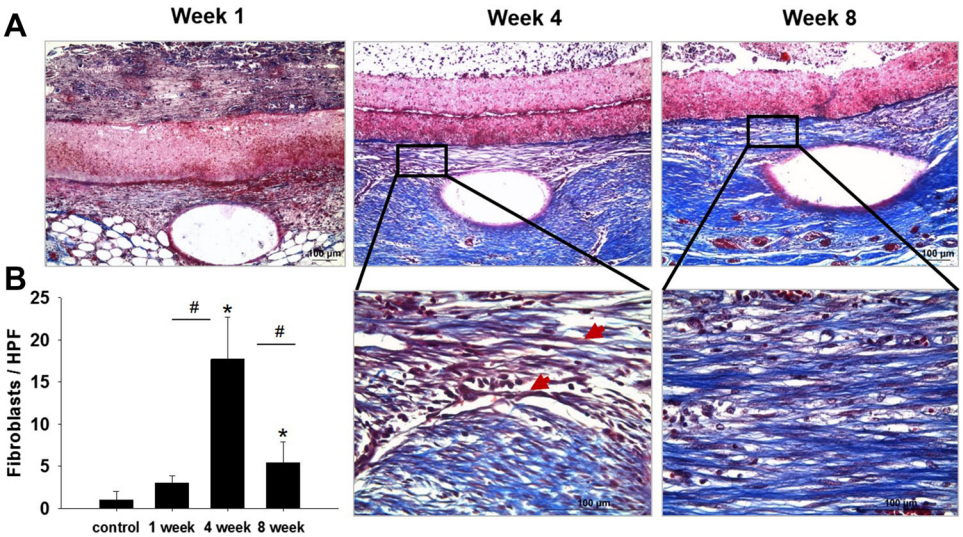

Fig. 5 **A** Masson's trichrome staining showed fibroblast infiltration at week 4 and increased collagen deposition at week 8. Fibroblasts and collagen were present in all animals, mainly organizing around the tracheal scaffold over time. A significant fibroproliferative response with deposition of fibroblasts (*arrows*) was seen at week 4. The *black box* indicates the magnified area. **B** Average number of fibroblasts per high-powered field (HPF) was quantified. Fibroblast count was performed in 5 HPF per tissue section (400x). Data are expressed as means ± SD. $*p < 0.05$, compared to the control group; $\#p < 0.05$ compared to 4 weeks; Mann–Whitney *U* test. *Scale bar* = 100 μm

to—and even death of patients [26]. The present study was performed to advance tracheal regeneration research by tracing and analyzing the causes of stenosis. In this study, we confirmed a very strong fibrotic reaction, as a result of the inflammatory response, especially at the anastomosis site. It is likely that the severe inflammatory reaction occurred in response to microorganisms introduced from the external environment during respiration, as well as to the scaffold itself. Inhaled air contains numerous bacteria, viruses, and microparticles [27] that can induce continuous inflammation until mucosal regeneration has completed at the inner lining of the transplanted trachea. The inflammatory response could also occur as a host innate response to scaffolds and sutures. Therefore, inflammation and

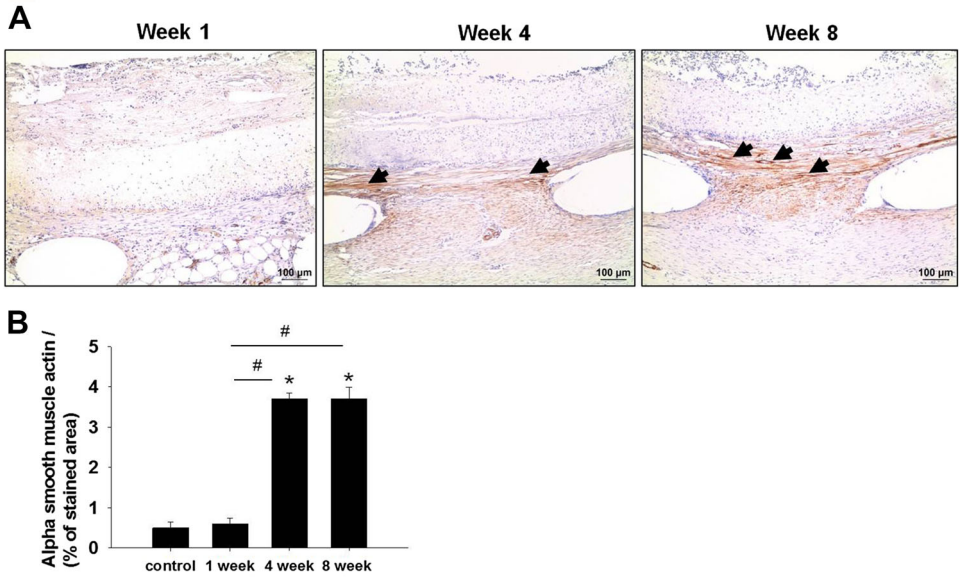

Fig. 6 Evaluation of the degree of α-smooth muscle actin (α-SMA) deposition. **A** Expression of α-SMA visualized by immunohistochemistry at 1, 4 and 8 weeks after implantation (*arrows*). **B** There was no difference in the intensity of immunohistochemical staining between week 4 and week 8. Data are expressed as means ± SD. $*p < 0.05$, compared to the control group; $\#p < 0.05$ compared to week 1; Mann–Whitney *U* test. *Scale bar* = 100 μm

resultant stenosis may be reduced if the mucosal lining inside the tracheal prosthesis is completed as soon as possible and the implanted scaffold and suture material are modified to avoid inducing an inflammatory reaction.

All implanted materials induce a foreign body reaction, which is primarily mediated by polymorphonuclear leukocytes and macrophages. The severity of reaction may depend on the nature of the implanted material, its structure, and surface topography [8, 9, 28, 29]. During the acute phase of the foreign body reaction, circulating polymorphonuclear leukocytes (neutrophils) are stimulated in response to inflammatory signals released at the tracheal implant site. Short-lived neutrophils are then replaced by inflammatory monocytes and macrophages. Macrophages are considered one of the key mediators of tracheal implant-associated inflammation due to their distribution and motility, and they generate a multitude of biologically active products. Macrophage, which play central roles in directing both inflammatory and regenerative responses associated with implanted biomaterials, can be classified into "classical" (M1) and "alternative" (M2) states of activation according to the cytokines produced [30]. Prototypic M1 macrophages are characterized by elevated production of proinflammatory cytokines, such as TNF-α, IL-1β, IL-6, and IL-12. In contrast, prototypic M2 macrophages are characterized by increased production of transforming growth factor-beta (TGF-β) and anti-inflammatory factors, such as IL-10 and IL-1Ra [31, 32]. M2 macrophages generate an anti-inflammatory environment and promote healing and regeneration of wounds. However, when the lesion is persistent, M2 macrophages play an important profibrotic role, and this cell population is known to secrete large amounts of profibrotic factors, such as TGF-β and Galactin-3 [33].

Fibrosis is a common consequence of chronic inflammation, developing as a result of failed wound healing. Fibrosis is induced by migration of fibroblasts to the site of implantation with proliferation and secretion of ECM components, such as collagen, fibronectin, and proteoglycan. Fibroblast activation is induced by various stimuli that arise when tissue injury occurs, including growth factors, such as TGF-β, epidermal growth factor (EGF), platelet-derived growth factor (PDGF), and fibroblast growth factor 2 (FGF-2), which are released by the surrounding tissue and infiltrating mononuclear cells [34–37]. Moreover, activated fibroblasts express α-SMA, leading to the term "myofibroblasts" [38]. The actin produced may distort the shape of the organ where it is deposited.

The relative time course of inflammatory cell recruitment to sites of damaged tissue may be classified into three stages: inflammation, proliferation/migration, and maturation/remodeling. Different types of cells are abundant in each stage; in the inflammatory phase, neutrophils are highly abundant. In the present study, neutrophils were observed in the highest numbers in the first week, and then decreased over time. These observations indicated that the inflammatory response occurred within 7 days of the operation. During the fourth week, the numbers of monocytes/macrophages increased with time, and migration of fibroblasts was observed. The percentage of monocytes/macrophages was highest during the eighth week. This can be understood as fibrosis beginning during the proliferation/migration phase and being an ongoing process. As a result of the fibrosis process, collagen deposition

was observed during the eighth week. This change in tissue configuration was similar to the typical fibrosis stage with much more stronger reaction than any other places. This stronger reaction is thought to be the result of the continuous exposure to pathogens inhaled through the airway.

The prevention of chronic inflammation or implant-associated infections by manipulating neutrophil migration or macrophage phenotype is a promising strategy to improve implant survival. Localized delivery of immunomodulatory factors is emerging as a strategy for controlling the recruitment of inflammatory cells around the implant site. Some cytokines, such as TGF-β, play significant roles in innate immunity, regulating the recruitment, activation, and function of neutrophils, macrophages, and natural killer (NK) cells [39]. Furthermore, TGF-β antagonizes antigen presentation function and maturation of dendritic cells [40]. Therefore, immunomodulatory cytokines and antibiotics bound to and slowly released from the tracheal scaffold may have roles in suppressing the immune reaction at the implant site and preventing fibrosis and restenosis [41–43]. Further studies to clarify the role of cytokines in tracheal regeneration are required, which may enable long-term successful clinical trials of tracheal implants.

In conclusion, serial analysis of leukocyte infiltration into tracheal scaffolds revealed significant increases in neutrophils at the first week and macrophages after the fourth week. Fibroblast recruitment was followed by α-SMA deposition and restenosis of the transplanted scaffold. The approach of locally controlling inflammation after biomaterial implantation may be an ideal target to enhance the long-term patency of tracheal engraftment.

Acknowledgements This research was supported by a grant of the Korea Health Technology R&D Project through the Korea Health Industry Development Institute (KHIDI), funded by the Ministry of Health & Welfare, Republic of Korea (Grant Number: HI14C0184 to S. K. K), by a Grant from the Seoul National University Hospital Research Fund (Grant Number: 0320140360 to S. K. K) and by the Education and Research Encouragement Fund of the Seoul National University Hospital (2016, to H. W. S).

Compliance with ethical standards

Conflicts of interest The authors declare no conflict of interest.

Ethical standard All protocols were performed in accordance with the guidelines of the Animal Care Ethics Committee of Seoul National University Hospital (IACUC No. 15-0268-C1A1).

References

1. Hagberg C, Georgi R, Krier C. Complications of managing the airway. Best Pract Res Clin Anaesthesiol. 2005;19:641–59.
2. Wain JC Jr. Postintubation tracheal stenosis. Semin Thorac Cardiovasc Surg. 2009;21:284–9.
3. Daumerie G, Su S, Ochroch EA. Anesthesia for the patient with tracheal stenosis. Anesthesiol Clin. 2010;28:157–74.
4. Shapshay SM, Beamis JF Jr, Hybels RL, Bohigian RK. Endoscopic treatment of subglottic and tracheal stenosis by radial laser incision and dilation. Ann Otol Rhinol Laryngol. 1987;96:661–4.
5. Lee KE, Shin JH, Song HY, Kim SB, Kim KR, Kim JH. Management of airway involvement of oesophageal cancer using covered retrievable nitinol stents. Clin Radiol. 2009;64:133–41.
6. Perepelitsyn I, Shapshay SM. Endoscopic treatment of laryngeal and tracheal stenosis-has mitomycin C improved the outcome? Otolaryngol Head Neck Surg. 2004;131:16–20.
7. Tatekawa Y, Kawazoe N, Chen G, Shirasaki Y, Komuro H, Kaneko M. Tracheal defect repair using a PLGA-collagen hybrid scaffold reinforced by a copolymer stent with bFGF-impregnated gelatin hydrogel. Pediatr Surg Int. 2010;26:575–80.
8. Lee DY, Lee JH, Ahn HJ, Oh SH, Kim TH, Kim HB, et al. Synergistic effect of laminin and mesenchymal stem cells on tracheal mucosal regeneration. Biomaterials. 2015;44:134–42.
9. Kwon SK, Song JJ, Cho CG, Park SW, Kim JR, Oh SH, et al. Tracheal reconstruction with asymmetrically porous polycaprolactone/pluronic F127 membranes. Head Neck. 2014;36:643–51.
10. Lee DY, Park SA, Lee SJ, Kim TH, Oh SH, Lee JH, et al. Segmental tracheal reconstruction by 3D-printed scaffold: pivotal role of asymmetrically porous membrane. Laryngoscope. 2016;126:E304–9.
11. Kim DH, Choi CB, Yang WJ, Chung WH, Lee AJ, Chung DJ, et al. Tracheal replacement with fresh and cryopreserved aortic allograft in adult dog. J Surg Res. 2012;175:199–206.
12. Makris D, Holder-Espinasse M, Wurtz A, Seguin A, Hubert T, Jaillard S, et al. Tracheal replacement with cryopreserved allogenic aorta. Chest. 2010;137:60–7.
13. Gonfiotti A, Jaus MO, Barale D, Baiguera S, Comin C, Lavorini F, et al. The first tissue-engineered airway transplantation: 5-year follow-up results. Lancet. 2014;383:238–44.
14. Eardley KS, Zehnder D, Quinkler M, Lepenies J, Bates RL, Savage CO, et al. The relationship between albuminuria, MCP-1/CCL2, and interstitial macrophages in chronic kidney disease. Kidney Int. 2006;69:1189–97.
15. Lech M, Anders HJ. Macrophages and fibrosis: how resident and infiltrating mononuclear phagocytes orchestrate all phases of tissue injury and repair. Biochim Biophys Acta. 2013;1832:989–97.
16. Hinz B, Phan SH, Thannickal VJ, Galli A, Bochaton-Piallat ML, Gabbiani G. The myofibroblast: one function, multiple origins. Am J Pathol. 2007;170:1807–16.
17. Rockey DC, Housset CN, Friedman SL. Activation-dependent contractility of rat hepatic lipocytes in culture and in vivo. J Clin Invest. 1993;92:1795–804.
18. Tacke F, Zimmermann HW. Macrophage heterogeneity in liver injury and fibrosis. J Hepatol. 2014;60:1090–6.
19. Hinz B, Celetta G, Tomasek JJ, Gabbiani G, Chaponnier C. Alpha-smooth muscle actin expression upregulates fibroblast contractile activity. Mol Biol Cell. 2001;12:2730–41.
20. Lee SJ, Heo DN, Moon JH, Park HN, Ko WK, Bae MS, et al. Chitosan/polyurethane blended fiber sheets containing silver sulfadiazine for use as an antimicrobial wound dressing. J Nanosci Nanotechnol. 2014;14:7488–94.
21. Lee SJ, Heo DN, Moon JH, Ko WK, Lee JB, Bae MS, et al. Electrospun chitosan nanofibers with controlled levels of silver nanoparticles. Preparation, characterization and antibacterial activity. Carbohydr Polym. 2014;111:530–7.
22. Lee SJ, Heo DN, Park JS, Kwon SK, Lee JH, Kim WD, et al. Characterization and preparation of bio-tubular scaffolds for fabricating artificial vascular grafts by combining electrospinning and a 3D printing system. Phys Chem Chem Phys. 2015;17:2996–9.

23. Elliott MJ, De Coppi P, Speggiorin S, Roebuck D, Butler CR, Samuel E, et al. Stem-cell-based, tissue engineered tracheal replacement in a child: a 2-year follow-up study. Lancet. 2012;380:994–1000.
24. Bacon JL, Patterson CM, Madden BP. Indications and interventional options for non-resectable tracheal stenosis. J Thorac Dis. 2014;6:258–70.
25. Macchiarini P, Jungebluth P, Go T, Asnaghi MA, Rees LE, Cogan TA, et al. Clinical transplantation of a tissue-engineered airway. Lancet. 2008;372:2023–30.
26. Berg M, Ejnell H, Kovacs A, Nayakawde N, Patil PB, Joshi M, et al. Replacement of a tracheal stenosis with a tissue-engineered human trachea using autologous stem cells: a case report. Tissue Eng A. 2014;20:389–97.
27. Park DU, Yeom JK, Lee WJ, Lee KM. Assessment of the levels of airborne bacteria, Gram-negative bacteria, and fungi in hospital lobbies. Int J Environ Res Public Health. 2013;10:541–55.
28. Du XF, Kwon SK, Song JJ, Cho CG, Park SW. Tracheal reconstruction by mesenchymal stem cells with small intestine submucosa in rabbits. Int J Pediatr Otorhinolaryngol. 2012;76:345–51.
29. Suzuki T, Kobayashi K, Tada Y, Suzuki Y, Wada I, Nakamura T, et al. Regeneration of the trachea using a bioengineered scaffold with adipose-derived stem cells. Ann Otol Rhinol Laryngol. 2008;117:453–63.
30. Braga TT, Agudelo JS, Camara NO. Macrophages during the fibrotic process: M2 as friend and foe. Front Immunol. 2015;6:602.
31. Kzhyshkowska J, Gudima A, Riabov V, Dollinger C, Lavalle P, Vrana NE. Macrophage responses to implants: prospects for personalized medicine. J Leukoc Biol. 2015;98:953–62.
32. Arango Duque G, Descoteaux A. Macrophage cytokines: involvement in immunity and infectious diseases. Front Immunol. 2014;5:491.
33. Vernon MA, Mylonas KJ, Hughes J. Macrophages and renal fibrosis. Semin Nephrol. 2010;30:302–17.
34. Antoniades HN, Bravo MA, Avila RE, Galanopoulos T, Neville-Golden J, Maxwell M, et al. Platelet-derived growth factor in idiopathic pulmonary fibrosis. J Clin Invest. 1990;86:1055–64.
35. Cowper SE, Bucala R. Nephrogenic fibrosing dermopathy: suspect identified, motive unclear. Am J Dermatopathol. 2003;25:358.
36. Munger JS, Huang X, Kawakatsu H, Griffiths MJ, Dalton SL, Wu J, et al. The integrin alpha v beta 6 binds and activates latent TGF beta 1: a mechanism for regulating pulmonary inflammation and fibrosis. Cell. 1999;96:319–28.
37. Chaudhary NI, Roth GJ, Hilberg F, Muller-Quernheim J, Prasse A, Zissel G, et al. Inhibition of PDGF, VEGF and FGF signalling attenuates fibrosis. Eur Respir J. 2007;29:976–85.
38. Wynn TA. Cellular and molecular mechanisms of fibrosis. J Pathol. 2008;214:199–210.
39. Yang L, Pang Y, Moses HL. TGF-beta and immune cells: an important regulatory axis in the tumor microenvironment and progression. Trends Immunol. 2010;31:220–7.
40. Kobie JJ, Wu RS, Kurt RA, Lou S, Adelman MK, Whitesell LJ, et al. Transforming growth factor beta inhibits the antigen-presenting functions and antitumor activity of dendritic cell vaccines. Cancer Res. 2003;63:1860–4.
41. Park S, Park M, Kim BH, Lee JE, Park HJ, Lee SH, et al. Acute suppression of TGF-ss with local, sustained release of tranilast against the formation of fibrous capsules around silicone implants. J Control Release. 2015;200:125–37.
42. Kim YK, Que R, Wang SW, Liu WF. Modification of biomaterials with a self-protein inhibits the macrophage response. Adv Healthc Mater. 2014;3:989–94.
43. Ozcelik H, Vrana NE, Gudima A, Riabov V, Gratchev A, Haikel Y, et al. Harnessing the multifunctionality in nature: a bioactive agent release system with self-antimicrobial and immunomodulatory properties. Adv Healthc Mater. 2015;4:2026–36.